AGU ADVANCING EARTH AND SPACE SCIENCE

Geophysical Research Letters

RESEARCH LETTER
10.1029/2020GL088429

The Influence of Warming Patterns on Passive Ocean Heat Uptake

Emily Newsom[1], **Laure Zanna**[1,2], **Samar Khatiwala**[3], **and Jonathan M. Gregory**[4,5]

[1]Atmospheric, Oceanic and Planetary Physics, University of Oxford, Oxford, UK, [2]Courant Institute of Mathematical Sciences, New York University, New York, NY, USA, [3]Department of Earth Sciences, University of Oxford, Oxford, UK, [4]National Centre for Atmospheric Science, University of Reading, Reading, UK, [5]Met Office Hadley Centre, Exeter, UK

Key Points:
- CMIP5-average sea surface temperature patterns damp passive ocean heat uptake efficiency by 24%
- Variations in surface warming patterns between models do not explain the spread in ocean heat uptake efficiency
- The spread in ocean heat uptake efficiency likely stems from differences in ocean circulation across CMIP5

Supporting Information:
- Supporting Information S1

Correspondence to:
E. Newsom,
emily.newsom@physics.ox.ac.uk

Citation:
Newsom, E., Zanna, L., Khatiwala, S., & Gregory, J. M. (2020). The influence of warming patterns on passive ocean heat uptake. *Geophysical Research Letters*, *47*, e2020GL088429. https://doi.org/10.1029/2020GL088429

Received 15 APR 2020
Accepted 19 AUG 2020
Accepted article online 25 AUG 2020

Abstract The climate's response to forcing depends on how efficiently heat is absorbed by the ocean. Much, if not most, of this ocean heat uptake results from the passive transport of warm surface waters into the ocean's interior. Here we examine how geographic patterns of surface warming influence the efficiency of this passive heat uptake process. We show that the average pattern of surface warming in CMIP5 damps passive ocean heat uptake efficiency by nearly 25%, as compared to homogeneous surface warming. This "pattern effect" occurs because strong ventilation and weak surface warming are robustly colocated, particularly in the Southern Ocean. However, variations in warming patterns across CMIP5 do not drive significant ensemble spread in passive ocean heat uptake efficiency. This spread is likely linked to intermodel differences in ocean circulation, which our idealized results suggest may be dominated by differences in Southern Ocean and subtropical ventilation processes.

1. Introduction

After a change in radiative forcing, surface warming is mitigated by the slow heating of the global ocean for centuries. The climate's adjustment during this period is often described heuristically by a simple linear energy-balance model (Andrews et al., 2012; Gregory et al., 2004):

$$\overline{N} = \overline{F} - \lambda \overline{T}. \tag{1}$$

Here, N, F, and T are the top-of-atmosphere (TOA) radiative imbalance perturbation, radiative forcing perturbation, and surface temperature anomaly, all defined with reference to an initial steady state, and the overbar denotes a global mean. The parameter λ represents the strength of global radiative feedback. Since the great majority of this radiative imbalance is absorbed by the ocean, it is common to equate $\overline{N}$ with the global mean rate of ocean heat uptake (OHU, where its global mean is $\overline{\mathrm{OHU}}$) (Cubasch et al., 2001; Raper et al., 2002), emphasizing the role $\overline{\mathrm{OHU}}$ plays in pacing surface warming.

Ocean heat uptake is the result of many dynamic and interactive processes such as advection, diffusion, and vertical mixing (Gregory, 2000). "Passive" ocean heat uptake (henceforth OHU_p) refers to the transport of surface temperature anomalies into the interior by the climatological (time mean) of these transport processes (and is sometimes called "added heat" Bouttes et al., 2014). Passive ocean heat uptake thus describes the component of OHU in which heat acts like a passive tracer. In truth, heat is not a passive tracer—its uptake, along with other processes such as wind changes, alters advection and mixing and redistributes existing background temperature gradients. This "redistributed" heat (Garuba & Klinger, 2016) can significantly influence the spatial distribution of ocean warming and, indirectly, $\overline{\mathrm{OHU}}$ (e.g., Banks & Gregory, 2006), particularly through changes in the North Atlantic (Bouttes et al., 2014; Garuba & Klinger, 2016; Rugenstein et al., 2013; Winton et al., 2013; Xie & Vallis, 2012). However, more recent studies argue that redistribution plays a small role, as compared to OHU_p, in setting global $\overline{\mathrm{OHU}}$ (Armour et al., 2016; Garuba & Klinger, 2018; Gregory, Bouttes, et al., 2016; Todd et al., 2020). Further, Bronselaer and Zanna (2020) find that the pattern of heat storage is increasingly determined by OHU_p as the anomalous heat content in the ocean grows.

These studies motivate deeper investigation into the processes governing passive ocean heat uptake and its relevance over the coming century. Here we will specifically focus on the influence of spatial patterns

of surface warming on OHU_p, motivated by the critical role warming patterns play in pacing the atmosphere's radiative response to forcing. Specifically, radiative feedbacks vary strongly in space, such that their collective global effect, that is, λ in Equation 1, depends sensitively on *where* surface warming occurs (Armour et al., 2013; Rose et al., 2014) through both local and nonlocal effects (Andrews et al., 2015; Bloch-Johnson et al., 2020; Ceppi & Gregory, 2019; Dong et al., 2019; Gregory & Andrews, 2016; Stuecker et al., 2018). This is termed a "pattern effect" (Stevens et al., 2016; Xie, 2020), whereby $\overline{N}$ depends not only on $\overline{T}$ (i.e., Equation 1) but also on its spatial pattern (i.e., $T(x, y)$). This effect operates only because *both* warming and radiative feedbacks vary geographically. Passive ocean heat uptake processes, specifically the advection and mixing that determine where the ocean is ventilated, have similarly rich spatial structure (Gebbie & Huybers, 2012; Khatiwala et al., 2012; Waugh et al., 2013). Possibly then, a pattern effect may also modulate $\overline{OHU_p}$. A natural metric for this effect is the "ocean heat uptake efficiency" (κ), which quantifies the global-mean rate of heat uptake per degree global surface warming, $\kappa = \overline{OHU}/\overline{T}$ (Gregory & Mitchell, 1997; Gregory, 2000; Winton et al., 2010). A pattern effect would be reflected by a change to κ through a spatial redistribution of the (equivalent) $\overline{T}$.

Here, we consider how sea surface warming patterns, specifically those driven by anthropogenic forcing, influence passive ocean heat uptake and uptake efficiency. We exploit an ensemble of CMIP5 simulations to characterize these patterns. Common across simulations, to varying degrees, is relatively minimal warming over the Southern and North Atlantic and relatively strong warming across the tropics and North Pacific (Figures 1 and S1 in the supporting information). Our primary goal is to understand how these shared characteristics contribute to the rate of passive ocean heat uptake and heat uptake efficiency, on average, across the ensemble. Our secondary goal is to understand if deviations in warming patterns across models contribute to differences in passive heat uptake and, specifically, to the substantial spread in κ identified in previous modeling ensembles (Kuhlbrodt & Gregory, 2012). For both, we use an idealized framework to emulate passive ocean heat uptake (e.g., Zanna et al., 2019).

2. Model and Methods

2.1. Sea Surface Warming in CMIP5

To isolate the sea surface temperature (SST) change in response to anthropogenic forcing, we examine the relatively idealized "1pctCO_2" forcing scenario in an ensemble of CMIP5 models. In these experiments, atmospheric carbon dioxide is increased from its preindustrial (late 19th century) concentration at a rate of 1% per year until doubled. We define the forced response as the change in SST in each perturbed simulation from that in a corresponding control simulation in which CO_2 is held constant at the preindustrial level. Here we will use the SST anomaly from each ensemble member as a boundary condition for passive heat uptake using two representations of a steady-state ocean circulation.

2.2. Green's Function Representations of the Ocean Circulation

In what follows, we use Green's functions (GFs) to extract the climatological time-mean (or "fixed") ocean circulation in two models. The first is the University of Victoria Earth System Climate Model (UVic ESCM) v2.9, a coupled climate model of intermediate complexity. UVic ESCM features a 3-D ocean general circulation model with a horizontal resolution of 1.8° × 3.6° and 19 layers that is coupled to a dynamic-thermodynamic sea ice, one-layer atmospheric energy-moisture balance and land surface models, as described by Muglia et al. (2018) and Khatiwala et al. (2019). The second is the Estimating the Circulation and Climate of the Ocean (ECCO)-Global Ocean Data Assimilation Experiment (GODAE), an ocean state estimate (Stammer et al., 2004; Wunsch & Heimbach, 2007) based on a 1° horizontal resolution configuration of MITgcm (Marshall et al., 1997) with 21 vertical layers. Both GFs were computed using the Transport Matrix Method (TMM) (Khatiwala et al., 2005, 2007, 2018), using monthly mean Transport Matrices and extracted from a monthly mean climatology over the 1992–2004 estimation period for ECCO. The Transport Matrices represent all transport processes in the underlying ocean model, including advection, mixing, and subgrid-scale parameterizations. For the GF simulations, we coarsen the surface into 26 surface patches for computational efficiency (see Zanna et al., 2019).

The GF for a given surface patch, j, or $G(j, r_i, t)$, quantifies how a passive tracer, present in patch j at time $t = 0$, will be dispersed over all interior points, r_i, by some later time t. Specifically, $G(j, r_i, t)$ is the solution at time t to a model's advection-diffusion equation with an impulse concentration surface boundary condition

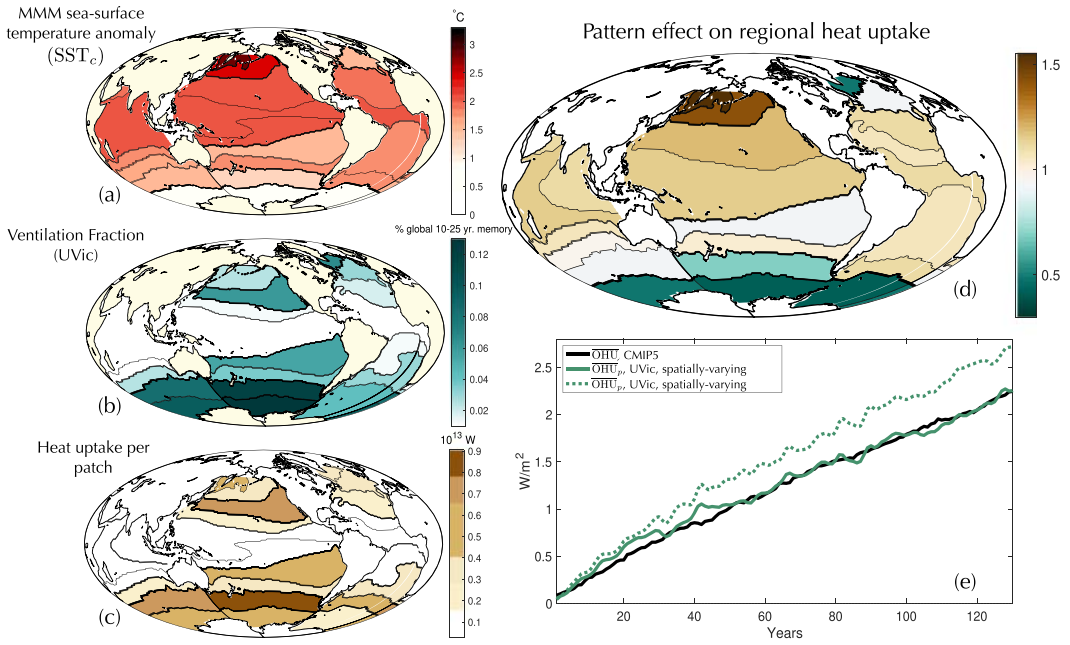

Figure 1. Summary of the pattern effect on passive ocean heat uptake. (a) Distribution of CMIP5 ensemble-mean sea surface temperature anomaly (ΔSST_c), averaged between years 100 and 140. (b) Comparison of $\overline{OHU}_p(t)$ for the spatially varying experiment (forced with the pattern ΔSST_c, green solid), spatially uniform experiment (forced everywhere at the same global mean rate, $\overline{\Delta SST}_c$, green dashed), as compared to the CMIP5 ensemble-mean $\overline{OHU}(t)$ (black solid). (c) Global ventilation fraction (VF) per patch, which is defined as $VF(j) = \int_0^\infty G_v(j,t)dt / \sum_{j=0}^{26} \int_0^\infty G_v(j,t)dt$ and is approximated here by truncating the time integral at 350 years. (d) Total heat uptake per patch (see Equation 4) averaged for years 100–140. This total uptake results from the covariance of ΔSST (a) and G_V (b). (e) Fraction of total patch heat uptake for the spatially varying experiment (OHU_p^{SV}) divided by patch uptake in the spatially uniform experiment (OHU_p^{SV}), or OHU_p^{SV}/OHU_p^{SU}.

at time 0 for points over patch j, and zero elsewhere and for $t > 0$ (Holzer & Hall, 2000; Khatiwala et al., 2001; Primeau, 2005). When integrated over all interior points, r_i, the GF

$$G_V(j,t) = \int_{V_i} G(j,r_i,t)d^3r_i,$$

quantifies the total fraction of waters last in contact with (ventilated from) patch j at $t = 0$ that remain in the interior at time t (Holzer & Hall, 2000; Khatiwala et al., 2012).

2.3. Passive Ocean Heat Uptake Using GFs

A GF representation of the ocean is particularly useful for emulating passive ocean heat uptake. Specifically, the global integral of heat passively absorbed (or, OHC_p, with the subscript p for "passive"), between an initial time $t = 0$, when the system is assumed to be in a steady state, and a later time t, due to the SST anomalies within patch j during that time interval is given by (e.g., Zanna et al., 2019)

$$OHC_p(j,t) = \rho_0 c_p \int_0^t \Delta SST(j,t')G_V(j,t-t')dt'. \quad (2)$$

Here, $\Delta SST(j,t)$ is the average SST anomaly over patch j at time t, and ρ_0 and c_p are a reference density and the heat capacity of seawater, respectively. Note that the heat sourced in each patch is dispersed throughout the ocean depending on local ventilation characteristics (i.e., G_V). The rate of passive ocean heat uptake per patch, $OHU_p(j,t)$, can thus be expressed as

$$OHU_p(j,t) = \frac{1}{A(j)}\frac{d}{dt}OHC_p(j,t) = \frac{\rho_0 c_p}{A(j)}\frac{d}{dt}\int_0^t \Delta SST(j,t)G_V(j,t-t')dt', \quad (3)$$

where $A(j)$ is the surface area of patch j. Given Equation 3, the area-weighted global-mean rate of passive ocean heat uptake, $\overline{\mathrm{OHU}}_p(t)$, then evolves as (e.g., Zanna et al., 2019)

$$\overline{\mathrm{OHU}}_p(t) = \frac{1}{A_g}\sum_{j=1}^{N}\underbrace{\mathrm{OHU}_p(j,t)A(j)}_{\text{total uptake per patch}}. \tag{4}$$

Here N is the number of surface patches (26 in this study), and $A_g = \sum_{j=1}^{N} A(j)$ is the global ocean area. The total uptake per patch represents the rate at which heat is conveyed from the surface layer into the interior from each patch, which is not necessarily the same location where the heat was fluxed across the sea surface. From Equation 4 we arrive at the "passive ocean heat uptake efficiency," defined as

$$\kappa_p(t) = \frac{\overline{\mathrm{OHU}_p}(t)}{\overline{T}(t)} = \frac{1}{A_g\overline{T}(t)}\sum_{j=1}^{N}\mathrm{OHU}_p(j,t)A(j),$$

where $\overline{T}$ is the global-mean surface air temperature anomaly, which in our case will be calculated from the same CMIP5 model that supplies our SST boundary conditions, as discussed below.

This framework is idealized and thus has limitations. First, we do not account for changes in ocean circulation and their influence on OHU. However, since we use SSTs from CMIP models, our approach does include the influence that circulation changes have on each model's SST anomalies, and hence indirectly on OHU, which is particularly important in the North Atlantic where AMOC weakening tends to cool the sea surface (e.g., Bouttes et al., 2014; Gregory, Bouttes, et al., 2016; Zanna et al., 2019). Second, our estimates will differ from the "true" passive heat uptake in a given CMIP model to the degree that our GFs differ from the coupled climate model's climatological circulation. Both these caveats stem from the fact that warming patterns are not actually independent of the circulation state; in reality, the circulation fundamentally influences OHU and thus, ΔSST, as discussed in sections 3.1,3.2, and 4. Finally, our discretization of the surface inevitably coarsens our representation of SST anomalies and ventilation pathways.

2.4. Experiments

We will use this framework for several sets of experiments, in which we simulate $\overline{\mathrm{OHU}}_p$ (Equation 4) using a suite of different ΔSST boundary conditions. We first test how the shared, or "characteristic", features of sea surface warming patterns across CMIP5 modulate $\overline{\mathrm{OHU}}_p$. To do so, we define the "characteristic" surface warming pattern as the CMIP5 ensemble-mean anomaly pattern, or $\Delta\mathrm{SST}_c(j,t)$. In section 3.1, we use $\Delta\mathrm{SST}_c$ as the surface boundary condition for our "spatially varying" experiment. We compare this with a "spatially uniform" experiment, where warming in each patch is equal and set to the global mean of $\Delta\mathrm{SST}_c(j,t)$, that is, $\Delta\mathrm{SST}(j,t) = \overline{\Delta\mathrm{SST}_c}(t) = \sum_{j=1}^{26}\Delta\mathrm{SST}_c(j,t)A(j)/A_g$. In both cases, κ_p will be calculated using the CMIP5 ensemble-mean surface air temperature anomaly. In section 3.2, we examine how variations in ΔSST patterns across CMIP5 impact the ensemble spread in $\overline{\mathrm{OHU}}_p$ and κ_p. To do so, we simulate a CMIP5 "counterpart" ensemble in which the ΔSST pattern from each individual CMIP5 model is used as the boundary condition for a corresponding GF simulation and $\overline{T}$ from each model will be used to calculate κ_p. All calculations are performed with both the UVic and ECCO GFs; however, we will focus on results from the UVic in section 3.1 for reasons discussed in section 3.2.

3. Results

3.1. Do Warming Patterns Influence the Average Passive Ocean Heat Uptake in CMIP5?

We first address how the characteristic warming pattern ($\Delta\mathrm{SST}_c$; Figure 1a) influences the rate of passive ocean heat uptake. To do so, we compare our spatially varying (in which the pattern $\Delta\mathrm{SST}_c$ used as the surface boundary condition) and spatially uniform experiments (in which the global mean of $\Delta\mathrm{SST}_c$ is used as the surface boundary condition everywhere; see section 2.4). Since these experiments share the same global-mean warming, differences between them will be due to the "pattern effect"—the influence that the geographic distribution of surface warming has on $\overline{\mathrm{OHU}}_p$, and thus on κ_p.

The evolution of $\overline{\mathrm{OHU}}_p(t)$ for each experiment, calculated with the UVic GF, is shown in Figure 1b, along with the CMIP5 ensemble-mean total heat uptake, $\overline{\mathrm{OHU}}$ (which includes all components of heat uptake,

including redistribution, depicted in black) over the same time period. Notably, $\overline{\mathrm{OHU}}_p$ and $\overline{\mathrm{OHU}}$ are in close agreement throughout the spatially varying (green solid) experiment. In contrast, the spatially uniform case (green dashed) overestimates $\overline{\mathrm{OHU}}$ by an average of 24%, exceeding it by 0.62 W m^{-2} during the final decade of the simulations. The pattern effect thus considerably damps the ocean's capacity to passively absorb heat. This damping is quantified by the reduction of κ_p from 0.73 W m^{-2} K^{-1} (spatially uniform) to 0.60 W m^{-2} K^{-1} (spatially varying), on average between years 60 and 130. Notably, when the pattern effect is accounted for, our idealized estimate closely resembles the CMIP5 ensemble mean of $\kappa = 0.62$ W m^{-2} K^{-1}.

What explains these differences? Generally, the amount of heat passively conveyed from the surface into the interior (Figure 1d) depends not only on regional SST's (i.e., Figure 1a), but also on the strength of regional ventilation. Figure 1c shows each patch's contribution to the global reservoir of all interior waters in the UVic GF (similar to the source fraction discussed by Khatiwala et al., 2012). In UVic, the Southern Ocean accounts for ≈66% of these waters, both because of ventilation by deep waters formed around Antarctic and by wind-driven subduction across subpolar latitudes. Despite convection in the North Atlantic, the region contributes only ~≈16% of this sequestered reservoir due to its small size (e.g., Khatiwala et al., 2012), roughly equaling contributions from the extratropical Pacific.

When imposed surface warming is spatially uniform, heat uptake patterns depend only on the ventilation pathways in our circulation model (Equation 3). Thus, the majority of heat is taken up in the Southern Ocean (2,060 ZJ total), while the North Atlantic and North Pacific account for only 365 and 195 ZJ, respectively (Figure S2a). In the spatially varying case, however, this partition differs significantly. The Southern Ocean and the North Atlantic absorb 57% and 17% less heat, respectively (Figures 1e and S2b). These differences result from the relatively minimal Southern Ocean and North Atlantic warming in $\Delta\mathrm{SST}_c$, with respect to the global mean, such that less heat can be conveyed downward despite equivalent ventilation rates. In the North Pacific, warming exceeds the global mean, driving an ≈55% increase in regional heat uptake (north of ≈40° N) to partially compensate reductions elsewhere. Strong tropical warming has little impact on global heat uptake (increasing $\overline{\mathrm{OHU}}_p$ by 3%)—warming patterns only modulate $\overline{\mathrm{OHU}}_p$ over ventilation regions. Note that, while the magnitude of heat uptake differs, the partition of relative regional contributions in our spatially varying experiment qualitatively resembles that estimated over the historical record by Zanna et al. (2019).

Critically, spatial patterns need not reduce $\overline{\mathrm{OHU}}_p$, a priori (see Equation 4). $\overline{\mathrm{OHU}}_p$ is damped in our experiments *only* because the coupled models, from which we calculate $\Delta\mathrm{SST}_c$, have less warming in regions where UVic ventilation is strong (most importantly the Southern Ocean) and more in regions where ventilation is considerably weaker (throughout the tropics, subtropics, and North Pacific). Note that vigorous UVic ventilation (Figure 1c) is collocated with regions of smaller ΔSST in the both the CMIP5 ensemble mean ($\Delta\mathrm{SST}_c$; Figure 1a) and in each ensemble member (Figure S1). For that reason, the pattern effect operates similarly if the same experiments are run using the ΔSST from each ensemble member instead of $\Delta\mathrm{SST}_c$ (see supplemental discussion and Figure S3). Physically, the broad-scale correspondence between strong ventilation (in UVic) and ΔSST patterns (in CMIP5) is evidence of the fundamental control ocean dynamics have on sea surface warming patterns. Specifically, the relatively minimal surface warming in the Southern Ocean and North Atlantic is, in large part, explained by the fact that models robustly ventilate in these regions, albeit at different rates (as discussed below) (Andrews et al., 2015; Armour et al., 2016; Marshall et al., 2014). Thus, the damping pattern effect, identified here by treating SST changes as independent of the circulation, operates precisely because ventilation acts as a regional thermostat on local SSTs, shaping warming patterns that, while variable (Figure S1), robustly involve reduced sea surface warming in ventilation regions. And because this general effect relies on broad-scale ventilation features shared across models, our results qualitatively hold regardless of the GF used—$\overline{\mathrm{OHU}}_p$ and κ_p are damped by ≈19% for the equivalent experiments using the ECCO GF, though their magnitudes are reduced because of different model dynamics as discussed below.

3.2. Do Warming Patterns Explain Differences Across CMIP5?

The average damping influence of warming patterns on κ_p, discussed above, is noteworthy in light of the substantial variations in both ΔSST patterns (Figure S1) and in κ across CMIP5 models (Figure 2b) (as well as in CMIP3; see Gregory & Forster, 2008). Do surface warming patterns explain this spread in κ? To test this possibility, we turn to our second set of experiments, the counterpart ensemble to CMIP5 calculated with fixed-circulation GFs (see section 2). The rate of global mean heat uptake (averaged for years 60–130)

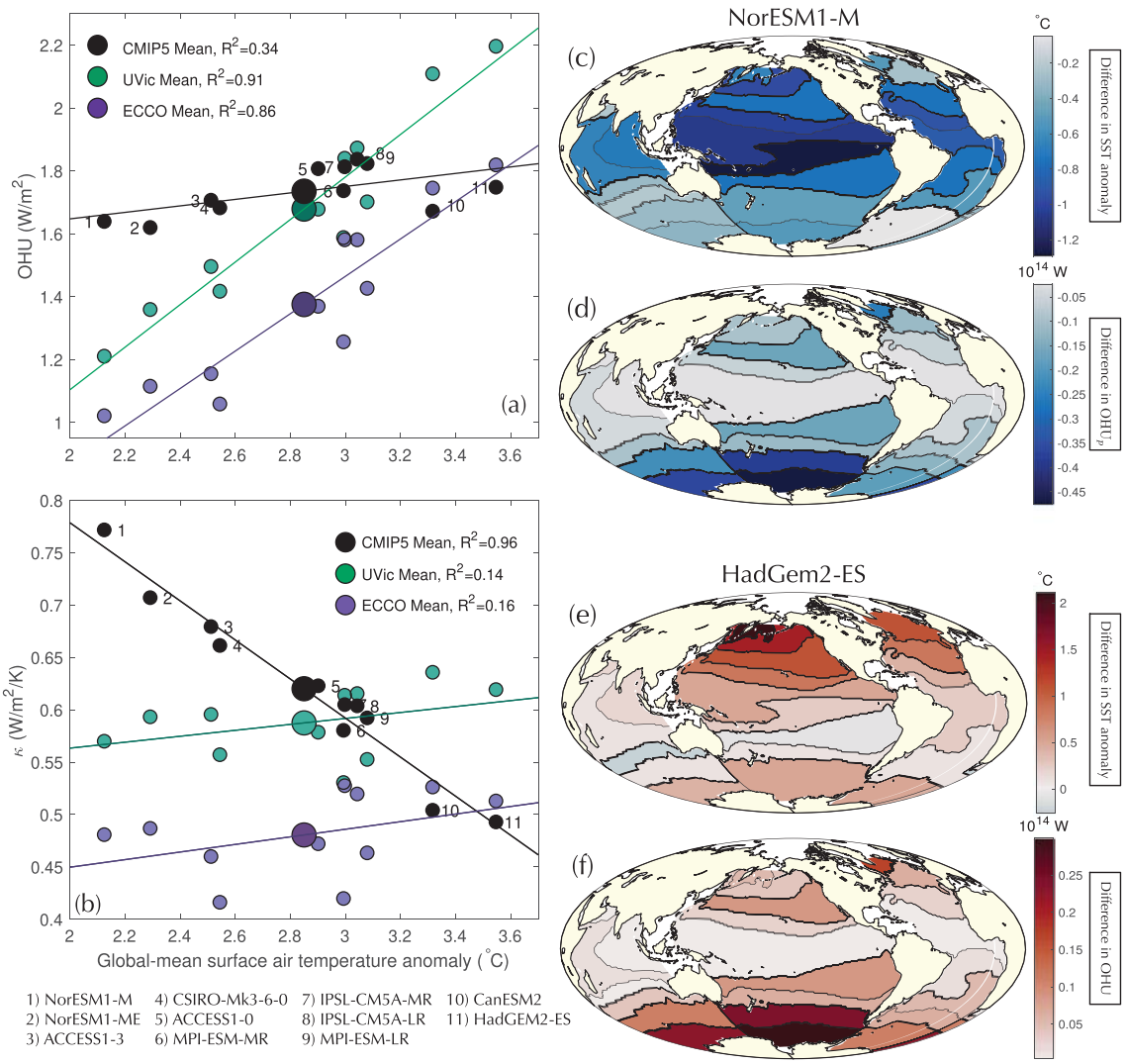

Figure 2. Variations in ocean heat uptake, ocean uptake efficiency, and surface warming between simulations. (a) $\overline{\text{OHU}}$ with global-mean surface air temperature anomaly, $\overline{T}$, for individual CMIP5 simulations (black). Each simulation's GF counterpart simulation, calculated with UVic (green) and the ECCO (purple), includes only passive heat uptake, $\overline{\text{OHU}}_p$. The mean value in each ensemble is also included (large circles). (b) κ for each CMIP 5 model (black) and (passive) κ_p for each GF counterpart simulation (UVic in green and ECCO in purple) with $\overline{T}$. In both, the ensemble-mean values are shown (large circles). (c) The difference in sea surface warming pattern in the coolest model outlier, NorESM1-M, from the CMIP5 ensemble-mean pattern (i.e., $\Delta\text{SST}_c(j,t) - \Delta\text{SST}_o(j,t)$, where "o" stands for outlier). (d) The associated anomaly in the total passive heat uptake per patch from the UVic ensemble-average pattern. (e) The same as (c) but for the warmest model outlier, HadGem2-ES; (f) the same as in (d) but for HadGem2-ES. Fields in all panels are averages over years 60–130 of the experiments.

is compared between GF ($\overline{\text{OHU}}_p$) and CMIP5 ($\overline{\text{OHU}}$) simulations in Figure 2a. Beginning with the UVic GF ensemble (green), $\overline{\text{OHU}}_p$ not only varies widely but also increases relatively linearly with the global-mean surface air temperature anomaly, $\overline{T}$, of the associated CMIP5 ensemble member (as would be anticipated from Equation 1 and the definition of κ). In contrast, there is comparatively little variation in $\overline{\text{OHU}}$ between CMIP5 models, such that the mismatch between each CMIP5 and GF simulation is greater for models in which $\overline{T}$ differs significantly from the ensemble mean. As a result, the spread in κ across CMIP5 models (Figure 2b, with std = 0.08 W m^{-2} K^{-1}) is largely set by variations in surface warming, such that κ decreases, also rather linearly, as $\overline{T}$ increases. The spread in κ_p across the GF ensemble is comparatively small (std = 0.03 W m^{-2} K^{-1})—variations in $\overline{\text{OHU}}_p$ are relatively proportional to those in $\overline{T}$ and thus largely cancel. Note that because of the linearity of our framework, the ensemble average of $\overline{\text{OHU}}_p$ is nearly equal to its value when forced with the ensemble-mean ΔSST_c (section 3.1), and similarly, the average κ in CMIP5.

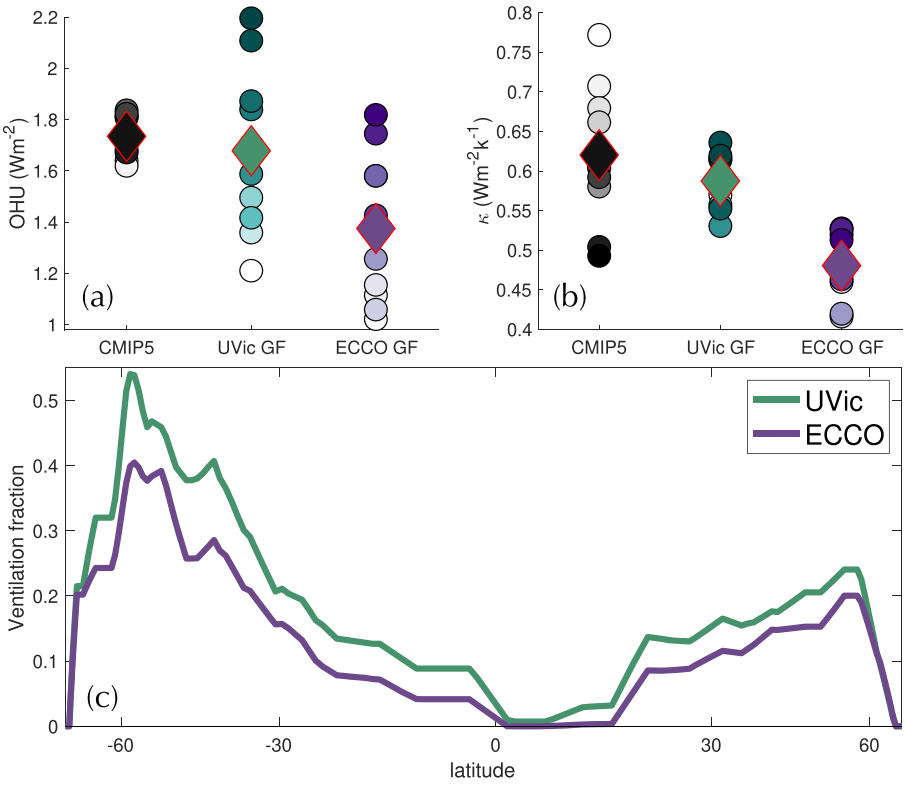

Figure 3. Effect of ventilation patterns on $\overline{\text{OHU}}$ and κ. (a) Spread in $\overline{\text{OHU}}$ for CMIP5 models (black) and in $\overline{\text{OHU}}_p$ for GF simulations using the UVic (green) and ECCO GFs (purple). Shading from light to dark indicates magnitude of surface warming, from cooler to warmer. Ensemble-mean values are overlaid (diamonds). (b) As in (a) but for κ (CMIP5) and κ_p (GFs). (c) The zonally summed ventilation fraction (VF) for UVic (green) and ECCO (purple). Fields are calculated as in Figure 1c, except $G_V(j,t)$ for both the UVic (G_V^U) and ECCO (G_V^E) are normalized by UVic global ventilation rates, thus for ECCO, $\text{VF}(j) = \int_0^\infty G_V^E(j,t)dt / \sum_{j=0}^{26} \int_0^\infty G_V^U(j,t)dt$. Doing so allows the comparison of the relative ventilation strength with latitude between GFs. Zonally summed VFs are smoothed by a Savitzky-Golay filter for visualization.

To understand why CMIP5 and GF simulations display different relationships to $\overline{T}$, we examine the coolest and warmest model outliers. While ΔSST patterns in each model are complex, these outliers share a common feature—extreme extratropical SST anomalies with respect to those in the ensemble-mean pattern ($\Delta\text{SST}_c(j,t)$). The two coolest models (NorESM1-M, Figure 2c, and NorESM1-ME, Figure S5c) both exhibit lower-than-average Southern Ocean, North Atlantic, and subtropical Pacific SST changes, as well as cooler equatorial regions. The corresponding GF simulations absorb less heat than average in these cases, primarily within the Southern Ocean, since relatively cool SSTs occur where the GF ventilates most vigorously (Figures 2d and S5d). We can further compare regional passive uptake estimates to the surface heat fluxes, though these metrics differ somewhat (as discussed in the supporting information). With this caveat, both GF simulations absorb less heat in the North Atlantic than is gained at the surface in their CMIP5 counterpart (59% and 65% less inNorESM1-ME and NorESM1-ME, respectively) while the coolest (NorESM1-M) takes up 22% less in the Southern Ocean as well (see Figures S4b and S4c), together explaining differences in $\overline{\text{OHU}}_p$ (GFs) and $\overline{\text{OHU}}$ (CMIP5).

The two warmest outliers generally exhibit the opposite behaviors. These models simulate above-average warming in the North Atlantic and Southern Oceans, as well as throughout the tropics (CanESM2; Figure S5e), and the North Pacific in the warmest outlier (in HADGEM2; Figure 2e). Again, warm anomalies occur in strong ventilation regions, so the GF simulations absorb significantly more heat than average, also primarily within the Southern Ocean (Figures 2f and S5f). In contrast to the coolest simulations, heat uptake exceeds regional CMIP5 surface fluxes foremost the Southern Ocean (by 45% in CanESM2 and 29% in HADGEM2) and secondarily the North Pacific, while both frameworks agree relatively well in the North Atlantic (Figures S4d and S4e). Together, these simulations clearly show that anomalously warm (or cool)

regional SST changes do not necessarily indicate greater (or lesser) regional heat uptake in CMIP5. They further show that the CMIP5 models that warm more (or less) globally also tend to warm more (or less) in extratropical ventilation regions. For that reason, OHU_p in a fixed-circulation model is constrained to increase with $\overline{T}$, a relationship that suppresses spread in κ_p.

Our results thus imply that a significant difference in κ_p must involve a difference in ventilation pathways, not just in surface boundary conditions. To test this implication, we compare the above results using UVic GF with those using the ECCO GF (see section 2). As in the UVic ensemble, $\overline{OHU}_p$ simulated with the ECCO GF increases quasi-linearly with $\overline{T}$ such that spread in κ_p remains relatively small with respect to CMIP5 (Figures 2 and 3). However, the ECCO GF systematically simulates lower $\overline{OHU}_p$ and thus has a lower κ_p for all experiments ($\kappa_p = 0.48$ W m^{-2} K^{-1} on average for years 60–130). Our linear framework allows us to quantify which regions underpin these differences. Both circulation models share the same broad-scale structure—both are primarily ventilated from the Southern Ocean (Figure 3c). However, despite differences in high-latitude processes—the ECCO, in fact, ventilates more vigorously from the North Atlantic (Figure S6)—differences in κ_p primarily arise from weaker subduction from across the subtropics and, most importantly, the Southern Ocean (north of ≈55° S; Figures 3 and S6). These regional differences support the conclusion of our idealized experiments (i.e., Figures 2a and 2b) that ventilation pathways strongly impact the global ocean heat uptake efficiency, particularly within the Southern Ocean. They also suggest that the ventilation characteristics of the UVic GF (when coarsened over these broad scales) are relatively representative of the ensemble mean in CMIP5. The correspondence between the rates of heat uptake in the CMIP5 ensemble mean and UVic (when forced with the CMIP5-mean surface warming pattern) would be otherwise hard to explain given the strong control ventilation pathways play in constraining OHU_p, demonstrated in Figures 2 and 3 and, in fact, given by Equations 2–4. However, similarities between the average ventilation in CMIP5 and the UVic GF are difficult to directly confirm.

4. Discussion

In this study, we investigated controls on the passive ocean heat uptake and passive ocean heat uptake efficiency. We found that the average spatial patterns of sea surface warming in CMIP5 significantly damp passive global ocean heat uptake and uptake efficiency (both by about 24%) in our idealized emulations of CMIP5. This "pattern effect" unfolds because of the characteristically minimal warming over regions that ventilate the ocean's interior. Critically, to identify this effect, our framework breaks the coupling between SST anomalies and the circulation. Yet the damping we show in fact operates *because* of the strong influence ocean dynamics exert on sea surface warming patterns in a coupled system. Specifically, reduced passive heat uptake in our experiments occurs because of relatively minimal surface warming over the Southern Ocean (the globally dominant ventilation region both in our models and in observations; see, e.g., Gebbie & Huybers, 2012; Khatiwala et al., 2012; Waugh et al., 2013) as well as over the North Atlantic. These robust characteristics of CMIP5 warming patterns emerge in part because all models ventilate in these regions, albeit at different rates (Andrews et al., 2015; Armour et al., 2016; Marshall et al., 2014). Thus, physically, this damping pattern effect operates because ventilation across CMIP5 (among other processes) suppresses strong warming in efficient ventilation regions, systematically eroding the ability of ventilation to passively convey heat into the interior (Figures 1 and S3).

When accounting for these ensemble-average patterns, our idealized and uncoupled UVic simulations almost perfectly recover the ensemble-average rate and magnitude of total heat uptake in CMIP5. This agreement holds both globally (Figure 1b) and within the Southern Ocean where the majority of passive heat uptake occurs (Figure S4). This correspondence is noteworthy, since our estimates do not account for dynamic ocean changes. Such changes have been found to significantly influence both regional and global heat uptake (e.g., Banks & Gregory, 2006; Garuba & Klinger, 2016; Gregory, 2000; Winton et al., 2010; Xie & Vallis, 2012), which likely explains disagreement in the North Atlantic surface heat fluxes and our uptake estimates (e.g., Bouttes et al., 2014; Zanna et al., 2019, as well as the supporting information and Figure S4). However, far less heat is taken up in the North Atlantic than the Southern Ocean in our estimates, in CMIP5, and in observations (Armour et al., 2016; Frölicher et al., 2015; Shi et al., 2018; Zanna et al., 2019), such that discrepancy in the North Atlantic does not drive significant global disagreement between frameworks. At the least, our experiments suggest that deep water formation and AMOC strength may play a smaller role in passive uptake than argued for by Boé et al. (2009) and Kostov et al. (2014). Instead, passive

heat uptake from the subtropical and northern Pacific may be more important than traditionally assumed (here contributing an average 20% of the global total in our experiments) due to the strong warming across these subduction regions. In sum, our results support the argument that passive heat uptake dominates total global heat uptake (Armour et al., 2016; Garuba & Klinger, 2018; Gregory, Bouttes, et al., 2016; Huber & Zanna, 2017; Todd et al., 2020; Zanna et al., 2019) particularly as the anomalous heat content in the ocean grows with sustained greenhouse forcing (Bronselaer & Zanna, 2020). If so, any effect that damps passive heat uptake, such as the pattern effect, will significantly reduce the ocean's capacity to sequester heat from the atmosphere.

Despite the important influence of the characteristic ensemble-mean warming pattern on the ensemble-mean behavior, we also show that variations in warming patterns among the models of the ensemble cannot explain the significant spread in their ocean heat uptake efficiency. In fact, perhaps surprisingly, the rate of global-mean ocean heat uptake is relatively constant across CMIP5 models. The ensemble spread in ocean heat uptake efficiency is instead predominately set by the spread in global-mean temperatures. However, when individual CMIP5 model's sea surface warming patterns are imposed upon fixed circulation models, heat uptake increases approximately linearly with global mean surface warming. This occurs because the CMIP5 models that warm more, globally, also tend to warm more in the extratropics where the fixed models ventilate, particularly within the Southern Ocean. Thus, in apparent contrast to CMIP5, the ocean heat uptake *efficiency* remains relatively constant when the circulation is fixed.

This demonstrates that the CMIP5 spread in efficiency must be driven by variations in ocean ventilation between models. That conclusion is reinforced by the substantial difference in global heat uptake efficiencies between the UVic and ECCO circulation models. The uptake efficiency is ≈23% higher in UVic because of its stronger Southern Ocean and subtropical ventilation, despite weaker North Atlantic ventilation. Since the UVic model captures the average efficiency in CMIP5 quite well (which implies that it may also emulate the large-scale, average circulation dynamics in CMIP5), it must therefore be an inferior emulator for those CMIP5 models in which ventilation dynamics vary widely from the ensemble mean (Figure 2).

Sea surface warming patterns are known to regulate the climate's transient response to forcing through their interaction with radiative feedbacks (Andrews et al., 2015; Armour et al., 2013; Bloch-Johnson et al., 2020; Ceppi & Gregory, 2019; Dong et al., 2019; Gregory & Andrews, 2016; Rose et al., 2014). Our results show that warming patterns additionally influence the climate response by damping the ocean's ability to absorb heat, on average, in coupled models. More generally, our results reinforce the growing consensus that understanding the coupled interplay between ocean ventilation, air-sea fluxes, and raditive feedbacks, which together shape emergent patterns of surface warming, is critical to improving climate change projections over the coming century (e.g., Forster et al., 2020; Gregory et al., 2020; Xie, 2020).

Data Availability Statement

Computing resources were provided by the University of Oxford Advanced Research Computing (ARC) facility (https://doi.org/10.5281/zenodo.22558) and the ARCHER UK National Supercomputing Service (http://www.archer.ac.uk). Transport Matrices for the ECCO-GOADE and UVic ESM used in this study are available online (at https://doi.org/10.5281/zenodo.1246300).

Acknowledgments
E. R. N., L. Z., and S. K.'s work was supported by NERC Project NE/P019218/1 on transient tracer-based Investigation of Circulation and Thermal Ocean Change (TICTOC). J. M. G.'s work was supported by NERC TICTOC Project NE/P019099/1. L. Z. and J. M. G.'s work also supported through NERC Grant NE/R000727/1 (UKFAFMIP). S. K. was also funded through U.S. NSF Grant OCE 12-34971 and UK NERC Grant NE/M020835/1.

References

Andrews, T., Gregory, J. M., & Webb, M. J. (2015). The dependence of radiative forcing and feedback on evolving patterns of surface temperature change in climate models. *Journal of Climate*, *28*(4), 1630–1648. https://doi.org/10.1175/JCLI-D-14-00545.1

Andrews, T., Gregory, J. M., Webb, M. J., & Taylor, K. E. (2012). Forcing, feedbacks and climate sensitivity in CMIP5 coupled atmosphere-ocean climate models. *Geophysical Research Letters*, *39*, L09712. https://doi.org/10.1029/2012GL051607

Armour, K. C., Bitz, C. M., & Roe, G. H. (2013). Time-varying climate sensitivity from regional feedbacks. *Journal of Climate*, *26*(13), 4518–4534. https://doi.org/10.1175/JCLI-D-12-00544.1

Armour, K. C., Marshall, J., Scott, J. R., Donohoe, A., & Newsom, E. R. (2016). Southern Ocean warming delayed by circumpolar upwelling and equatorward transport. *Nature Geoscience*, *9*(7), 549–554. https://doi.org/10.1038/ngeo2731

Banks, H. T., & Gregory, J. M. (2006). Mechanisms of ocean heat uptake in a coupled climate model and the implications for tracer based predictions of ocean heat uptake. *Geophysical Research Letters*, *33*, L07608. https://doi.org/10.1029/2005GL025352

Bloch-Johnson, J., Rugenstein, M., & Abbot, D. S. (2020). Spatial radiative feedbacks from internal variability using multiple regression. *Journal of Climate*, *33*(10), 4121–4140. https://doi.org/10.1175/jcli-d-19-0396.1

Boé, J., Hall, & Qu, X. (2009). Deep ocean heat uptake as a major source of spread in transient climate change simulations. *Geophysical Research Letters*, *36*, L22701. https://doi.org/10.1029/2009GL040845

Bouttes, N., Gregory, J. M., Kuhlbrodt, T., & Smith, R. S. (2014). The drivers of projected North Atlantic sea level change. *Climate Dynamics*, *43*(5-6), 1531–1544. https://doi.org/10.1007/s00382-013-1973-8

Bronselaer, B., & Zanna, L. (2020). Heat and carbon coupling reveals ocean warming due to circulation changes. *Nature*, *584*(January), 1–7. https://doi.org/10.1038/s41586-020-2573-5

Ceppi, P., & Gregory, J. M. (2019). A refined model for the Earth's global energy balance. *Climate Dynamics*, *53*(7-8), 4781–4797. https://doi.org/10.1007/s00382-019-04825-x

Cubasch, U., Meehl, G. A., Boer, G. J., Stouffer, R. J., Dix, M., Noda, A., et al. (2001). Chapter 9—Projections of future climate change. *Climate Change*, *2001*, 525–582.

Dong, Y., Proistosescu, C., Armour, K. C., & Battisti, D. S. (2019). Attributing historical and future evolution of radiative feedbacks to regional warming patterns using a Green's function approach: The preeminence of the western pacific. *Journal of Climate*, *32*(17), 5471–5491. https://doi.org/10.1175/jcli-d-18-0843.1

Forster, P. M., Maycock, A. C., McKenna, C. M., & Smith, C. J. (2020). Latest climate models confirm need for urgent mitigation. *Nature Climate Change*, *10*(1), 7–10. https://doi.org/10.1038/s41558-019-0660-0

Frölicher, T. L., Sarmiento, J. L., Paynter, D. J., Dunne, J. P., Krasting, J. P., & Winton, M. (2015). Dominance of the Southern Ocean in anthropogenic carbon and heat uptake in CMIP5 models. *Journal of Climate*, *28*(2), 862–886. https://doi.org/10.1175/JCLI-D-14-00117.1

Garuba, O. A., & Klinger, B. A. (2016). Ocean heat uptake and interbasin transport of the passive and redistributive components of surface heating. *Journal of Climate*, *29*(20), 7507–7527. https://doi.org/10.1175/JCLI-D-16-0138.1

Garuba, O. A., & Klinger, B. A. (2018). The role of individual surface flux components in the passive and active ocean heat uptake. *Journal of Climate*, *31*(15), 6157–6173. https://doi.org/10.1175/JCLI-D-17-0452.1

Gebbie, G., & Huybers, P. (2012). The mean age of ocean waters inferred from radiocarbon observations: Sensitivity to surface sources and accounting for mixing histories. *Journal of Physical Oceanography*, *42*(2), 291–305. https://doi.org/10.1175/JPO-D-11-043.1

Gregory, J. M. (2000). Vertical heat transports in the ocean and their effect on time-dependent climate change. *Climate Dynamics*, *16*, 501–515. https://doi.org/10.1007/s003820000059

Gregory, J. M., & Andrews, T. (2016). Variation in climate sensitivity and feedback parameters during the historical period. *Geophysical Research Letters*, *43*, 3911–3920. https://doi.org/10.1002/2016GL068406

Gregory, J. M., Andrews, T., Ceppi, P., Mauritsen, T., & Webb, M. J. (2020). How accurately can the climate sensitivity to CO_2 be estimated from historical climate change? *Climate Dynamics*, *54*(1–2), 129–157. https://doi.org/10.1007/s00382-019-04991-y

Gregory, J. M., Bouttes, N., Griffies, S. M., Haak, H., Hurlin, W. J., Jungclaus, J., et al. (2016). The Flux-Anomaly-Forced Model Pntercomparison Project (FAFMIP) contribution to CMIP6: Investigation of sea-level and ocean climate change in response to CO_2 forcing. *Geoscientific Model Development*, *9*(11), 3993–4017. https://doi.org/10.5194/gmd-9-3993-2016

Gregory, J. M., & Forster, P. M. (2008). Transient climate response estimated from radiative forcing and observed temperature change. *Journal of Geophysical Research*, *113*, D23105. https://doi.org/10.1029/2008JD010405

Gregory, J. M., Ingram, W. J., Palmer, M. A., Jones, G. S., Stott, P. A., Thorpe, R. B., et al. (2004). A new method for diagnosing radiative forcing and climate sensitivity. *Geophysical Research Letters*, *31*, L03205. https://doi.org/10.1029/2003GL018747

Gregory, J. M., & Mitchell, J. F. B. (1997). The climate response to CO_2 of the Hadley Centre coupled AOGCM with and without flux adjustment. *Geophysical Research Letters*, *24*(15), 1943–1946. https://doi.org/10.1029/97GL01930

Holzer, M., & Hall, T. M. (2000). Transit-time and tracer-age distributions in geophysical flows. *Journal of the Atmospheric Sciences*, *57*(21), 3539–3558. https://doi.org/10.1175/1520-0469(2000)057<3539:TTATAD>2.0.CO;2

Huber, M. B., & Zanna, L. (2017). Drivers of uncertainty in simulated ocean circulation and heat uptake. *Geophysical Research Letters*, *44*, 1402–1413. https://doi.org/10.1002/2016GL071587

Khatiwala, S. (2007). A computational framework for simulation of biogeochemical tracers in the ocean. *Global Biogeochemical Cycles*, *21*, GB3001. https://doi.org/10.1029/2007GB002923

Khatiwala, S. (2018). Transport Matrix Method software for ocean biogeochemical simulations. https://doi.org/10.5281/zenodo.1246300

Khatiwala, S., Primeau, F., & Holzer, M. (2012). Ventilation of the deep ocean constrained with tracer observations and implications for radiocarbon estimates of ideal mean age. *Earth and Planetary Science Letters*, *325–326*, 116–125. https://doi.org/10.1016/j.epsl.2012.01.038

Khatiwala, S., Schmittner, A., & Muglia, J. (2019). Air-sea disequilibrium enhances ocean carbon storage during glacial periods. *Science Advances*, *5*, 1–11.

Khatiwala, S., Visbeck, M., & Cane, M. A. (2005). Accelerated simulation of passive tracers in ocean circulation models. *Ocean Modelling*, *9*(1), 51–69. https://doi.org/10.1016/j.ocemod.2004.04.002

Khatiwala, S., Visbeck, M., & Schlosser, P. (2001). Age tracers in an ocean GCM. *Deep-Sea Research Part I: Oceanographic Research Papers*, *48*(6), 1423–1441. https://doi.org/10.1016/S0967-0637(00)00094-7

Kostov, Y., Armour, K. C., & Marshall, J. (2014). Impact of the Atlantic meridional overturning circulation on ocean heat storage and transient climate change. *Geophysical Research Letters*, *41*, 2108–2116. https://doi.org/10.1002/2013GL058998

Kuhlbrodt, T., & Gregory, J. M. (2012). Ocean heat uptake and its consequences for the magnitude of sea level rise and climate change. *Geophysical Research Letters*, *39*, L18608. https://doi.org/10.1029/2012GL052952

Marshall, J., Adcroft, A., Hill, C., Perelman, L., & Heisey, C. (1997). A finite-volume, incompressible Navier-Stokes model for studies of the ocean on parallel computers. *Journal of Geophysical Research*, *102*, 5733–5752.

Marshall, J., Armour, K. C., Scott, J. R., Kostov, Y., Hausmann, U., Ferreira, D., et al. (2014). The ocean's role in polar climate change: Asymmetric Arctic and Antarctic responses to greenhouse gas and ozone forcing. *Philosophical Transactions of the Royal Society A*, *372*, 20130040. https://doi.org/10.1098/rsta.2013.0040

Muglia, J., Skinner, L. C., & Schmittner, A. (2018). Weak overturning circulation and high Southern Ocean nutrient utilization maximized glacial ocean carbon. *Earth and Planetary Science Letters*, *496*, 47–56. https://doi.org/10.1016/j.epsl.2018.05.038

Primeau, F. (2005). Characterizing transport between the surface mixed layer and the ocean interior with a forward and adjoint global ocean transport model. *Journal of Physical Oceanography*, *35*, 545–564.

Raper, S. C., Gregory, J. M., & Stouffer, R. J. (2002). The role of climate sensitivity and ocean heat uptake on AOGCM transient temperature response. *Journal of Climate*, *15*, 124–130.

Rose, B. E. J., Armour, K. C., Battisti, D. S., Feldl, N., & Koll, D. D. B. (2014). The dependence of transient climate sensitivity and radiative feedbacks on the spatial pattern of ocean heat uptake. *Geophysical Research Letters*, *41*, 1071–1078. https://doi.org/10.1002/2013GL058955

Rugenstein, M., Winton, M., Stouffer, R. J., Griffies, S. M., & Hallberg, R. (2013). Northern high-latitude heat budget decomposition and transient warming. *Journal of Climate*, *26*(2), 609–621. https://doi.org/10.1175/JCLI-D-11-00695.1

Shi, J. R., Xie, S. P., & Talley, L. D. (2018). Evolving relative importance of the Southern Ocean and North Atlantic in anthropogenic ocean heat uptake. *Journal of Climate*, *31*(18), 7459–7479. https://doi.org/10.1175/JCLI-D-18-0170.1

Stammer, D., Ueyoshi, K., Köhl, A., Large, W. G., Josey, S. A., & Wunsch, C. (2004). Estimating air-sea fluxes of heat, freshwater, and momentum through global ocean data assimilation. *Journal of Geophysical Research*, *109*, C05023. https://doi.org/10.1029/2003JC002082

Stevens, B., Sherwood, S. C., Bony, S., & Webb, M. J. (2016). Prospects for narrowing bounds on Earth's equilibrium climate sensitivity. *Earth's Future*, *4*(11), 512–522. https://doi.org/10.1002/2016EF000376

Stuecker, M. F., Bitz, C. M., Armour, K. C., Proistosescu, C., Kang, S. M., Xie, S. P., et al. (2018). Polar amplification dominated by local forcing and feedbacks. *Nature Climate Change*, *8*(12), 1076–1081. https://doi.org/10.1038/s41558-018-0339-y

Todd, A., Zanna, L., Couldrey, M., Gregory, J. M., Wu, Q., Church, J. A., et al. (2020). Ocean-only FAFMIP: Understanding regional patterns of ocean heat content and dynamic sea level change. *Journal of Advances in Modeling Earth Systems*, *12*, e2019MS002027. https://doi.org/10.1002/essoar.10501557.1

Waugh, D., Primeau, F., DeVries, T., & Holzer, M. (2013). Recent changes in the ventilation of the southern oceans. *Science*, *339*(6119), 568–570. https://doi.org/10.1126/science.1225411

Winton, M., Griffies, S. M., Samuels, B. L., Sarmiento, J. L., & Frölicher, T. L. (2013). Connecting changing ocean circulation with changing climate. *Journal of Climate*, *26*(7), 2268–2278. https://doi.org/10.1175/JCLI-D-12-00296.1

Winton, M., Takahashi, K., & Held, I. M. (2010). Importance of ocean heat uptake efficacy to transient climate change. *Journal of Climate*, *23*(9), 2333–2344. https://doi.org/10.1175/2009JCLI3139.1

Wunsch, C., & Heimbach, P. (2007). Practical global oceanic state estimation. *Physica D*, *230*, 197–208.

Xie, S. P. (2020). Ocean warming pattern effect on global and regional climate change. *AGU Advances*, *1*(1), 1–7. https://doi.org/10.1029/2019AV000130

Xie, P., & Vallis, G. K. (2012). The passive and active nature of ocean heat uptake in idealized climate change experiments. *Climate Dynamics*, *38*, 667–684. https://doi.org/10.1007/s00382-011-1063-8

Zanna, L., Khatiwala, S., Gregory, J. M., Ison, J., & Heimbach, P. (2019). Global reconstruction of historical ocean heat storage and transport. *Proceedings of the National Academy of Sciences of the United States of America*, *116*(4), 1126–1131. https://doi.org/10.1073/pnas.1808838115